EPJ Web of Conferences **359**, 01004 (2026) https://doi.org/10.1051/epjconf/202635901004
ICEMR-2025

Synthesis, Structural Characterization, and Visible-Light-Driven Photocatalytic Activity of $DyFeO_3$ Nanoparticles

Noorjahan Begum V.S[1,2], and *Zarena* D[3],[*]

[1]Government College (A), Anantapur, AP., India
[2]Department of Physics, JNTUA College of Engineering, Anantapur -515002, Andhra Pradesh, India
[3]Department of Physics, Jawaharlal Nehru Technological University Anantapur, Anantapur - 515002, Andhra Pradesh, India

Abstract.

Single-phase $DyFeO_3$ nanoparticles with orthorhombic perovskite structure (space group Pbnm) were synthesized and characterized successfully using X-ray diffraction (XRD), Rietveld refinement, scanning electron microscopy (SEM), energy-dispersive X-ray (EDX) spectroscopy, and UV–Vis spectroscopy. Phase purity was confirmed by XRD analysis with lattice parameters a = 5.5631 Å, b = 7.8516 Å, and c = 5.5530 Å, and the average crystallite size of 136 nm. SEM showed non-isometric nanoparticles of approximately 123 nm size with some agglomeration, and EDX assured stoichiometric elemental composition and homogeneity. Optical investigations showed direct band gap of approximately 2.01 eV corresponding to O 2p → Fe 3d charge-transfer transitions. $DyFeO_3$ nanoparticles showed good photo catalytic activity under visible light, effectively degrading several organic dyes (AF, MB, RhB, MO) according to first-order kinetics, with the degradation rates dependent upon dye structure and adsorption affinity. These results illustrate that $DyFeO_3$ nanoparticles are structurally stable, optically active, and efficient visible-light-driven photo catalysts, pointing toward their future use in environmental remediation techniques.

Keywords: : X-ray diffraction, Rietveld refinement, UV–Vis spectroscopy, band gap, photocatalytic activity, organic dye degradation, visible-light photocatalyst.

1 Introduction

Rare-earth orthoferrites (RFeO3, where R = Dy, Gd, Eu, Tb, etc.) are a class of perovskite-type materials that have attracted significant attention due to their multifunctional properties, including magnetic, optical, ferroelectric, and catalytic behavior[1, 2]. Their orthorhombic perovskite structure allows strong interactions between the rare-earth A-site cations and transition metal B-site cations, resulting in versatile physical and chemical properties. Among these, $DyFeO_3$ is particularly promising owing to its high thermal stability, strong magnetic ordering, and tunable electronic structure[3, 4]. These properties make $DyFeO_3$ suitable for a range of contemporary applications, such as visible-light-driven photocatalysis for environmental remediation, magnetic sensors, spintronic devices, optoelectronic components, and energy storage in multifunctional devices[5, 6]. Various synthesis methods,

[*]e-mail: zareenajntua@gmail.com

including solid-state reactions, hydrothermal, co-precipitation, and sol–gel techniques, have been employed to fabricate RFeO3 nanoparticles with controlled size, morphology, and crystallinity. Among these, the sol–gel method is advantageous because it allows precise stoichiometric control, low processing temperature, and uniform particle size distribution, which are essential for optimizing structural and functional properties[7, 8]. Previous studies have largely focused on bulk or micrometer-scale $DyFeO_3$, but achieving nanoscale particles with high crystallinity, homogeneous elemental distribution, and enhanced surface area is crucial to improving optical absorption, charge separation, and photocatalytic efficiency. With the increasing demand for sustainable environmental technologies, the development of visible-light-active photocatalysts for the degradation of organic pollutants has become a critical research focus. $DyFeO_3$ nanoparticles, owing to their suitable band gap (2.0 eV) and orthorhombically distorted perovskite structure, can effectively harvest visible light and generate electron–hole pairs that drive oxidation–reduction reactions for pollutant degradation. Beyond environmental remediation, $DyFeO_3$ has attracted growing interest for advanced applications including next-generation spintronic devices, magneto-optical sensors, energy conversion systems, and flexible electronic devices[9, 10]. In this study, $DyFeO_3$ nanoparticles were synthesized via a sol–gel route, followed by comprehensive structural, morphological, and optical characterization, and systematic evaluation of their visible-light-driven photocatalytic performance toward various organic dyes, thereby demonstrating their multifunctional potential for both environmental and technological applications [11, 12].

2 Experimental Procedure

The $DyFeO_3$ nanoparticles were synthesized via a citrate-assisted sol–gel method using dysprosium nitrate hexahydrate ($Dy(NO_3)_3{\cdot}6H_2O$, 99.9%, Sigma-Aldrich) and ferric nitrate nonahydrate ($Fe(NO_3)_3{\cdot}9H_2O$, 99%, Sigma-Aldrich) as precursors, citric acid ($C_6H_8O_7{\cdot}H_2O$, 99.5%, Merck) as a complexing agent, and ethylene glycol ($C_2H_6O_2$, 99%, Merck) as a polycondensation agent. Stoichiometric amounts of $Dy(NO_3)_3{\cdot}6H_2O$ and $Fe(NO_3)_3{\cdot}9H_2O$ were dissolved in 100 mL deionized water under magnetic stirring at 60^0C for 30 min. Citric acid was added in a 1:2 molar ratio with respect to the metal ions, and ethylene glycol in a 1:1 ratio with citric acid. The mixture was stirred at 80^0C for 2 h to form a homogeneous gel, which was subsequently dried at 120^0C for 12 h in a hot-air oven to remove water and partially decompose organics, yielding a brown precursor powder. The powder was calcined at 700 ^{0}C for 4 h in a programmable muffle furnace (heating rate 5 ^{0}C/min) to obtain crystalline $DyFeO_3$ nanoparticles. X-ray diffraction (XRD) patterns were recorded on a Rigaku Ultima IV diffractometer using Cu Kα radiation (λ = 1.5406 Å) in the 2θ range of $10–80^0$ with a step size of 0.02^0 and a scan rate of 1^0/min, and Rietveld refinement was performed using the FullProf software to détermine lattice parameters and phase purity. Morphology and particle size were examined using a JEOL JSM-7600F scanning electron microscope (SEM), and elemental composition was analyzed via energy-dispersive X-ray (EDX) spectroscopy. UV–Vis absorption spectra were recorded on a PerkinElmer Lambda 35 spectrophotometer in the 200–800 nm range, and the direct band gap was estimated using Tauc's plot. Photocatalytic activity was evaluated by monitoring the degradation of four organic dyes methyl orange (MO), rhodamine B (RhB), methylene blue (MB), and acid fuchsine (AF) under visible light irradiation (300 W Xe lamp, $\lambda > 400$ nm) at room temperature, with a catalyst dosage of 1 g/L and dye concentration of 10 mg/L.

3 Results and Discussion

The X-ray diffraction (XRD) spectrum of the as-prepared $DyFeO_3$ particles is shown in Fig1, together with the standard XRD pattern of orthorhombic $DyFeO_3$ (JCPDS: 98-008-0866) [13]. The diffraction profile clearly shows the distinctive Bragg reflections of rare-earth orthoferrites, indicating the successful formation of crystalline, perovskite-structured nanomaterials. All the diffraction peaks are indexed to the $DyFeO_3$ phase, and no secondary impurity phase is observed. The calculated lattice parameters from the diffraction data are a = 5.5631 Å, b = 7.8516 Å, and c = 5.5530 Å. The strong diffraction peak at $2\theta = 32.23^0$ is due to the convolution of (200), (121), and (002) planes. The average crystallite size, as estimated based on the Debye–Scherrer formula at this peak, is 136 nm. Rietveld refinement was done under the assumption of an orthorhombic structure with space group Pbnm (D_{2h}^{16}) to establish the phase purity and the lack of secondary phases [14]. Fig1 presents the refined XRD pattern where the red solid line refers to the model calculated, the black dots refer to the experimental one, and the blue dashed line refers to the difference between observed and fitted profiles. The green vertical ticks indicate the positions of the Bragg peaks. The inset indicates the quality of the higher-order reflections fitting, which further supports the refinement. Results of the refinement, such as fitting parameters, atomic positions, and estimated lattice constants, are listed in Table 1. The quality factors of the refinement were achieved as RWP = 6.31 %, RP = 5.21 %, and $\chi^2 = 1.96$, reflecting an excellent fit between observed and calculated patterns. The values of the obtained measurements agree with earlier findings on rare-earth orthoferrites in both the micrometer and bulk regimes. The lattice distortion in $DyFeO_3$ is due to the reduced ionic radius of Dy^{3+} (coordination number = 8) as opposed to the ideal A-site cation of a cubic perovskite with a coordination number of 12. Such incompatibility, expressed as the ionic radius ratio $r(Fe^{3+})/r(Dy^{3+}) = 0.605$ instead of the ideal 0.56 (such as in $SrTiO_3$), results in a lack of cubic symmetry and stabilization of the orthorhombic perovskite structure. Notably, no second phases typically observed in rare-earth orthoferrites were found in

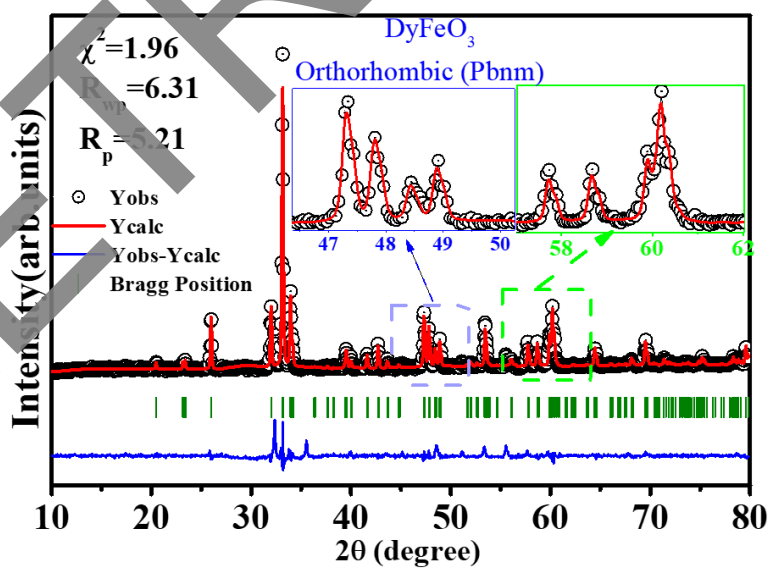

Figure 1. Rietveld refinement profiles of $DyFeO_3$ nano particle prepared with help of sol-gel method along with best fitting profiles

the current investigation, affirming the single-phase character of $DyFeO_3$.

Fig2 indicates the surface morphology of powder-synthesized $DyFeO_3$ nanoparticles with particles having size dispersion throughout the distribution. The nanoparticles are non-isometric in shape, and they have an average particle size of approximately 123 nm. There is evidence of agglomeration as the nanoparticles clump together because of their high surface energy and magnetic interactions. From the curve of the Gaussian distribution, the average particle size is 123 nm. EDX spectroscopy also verifies the elemental composition of the $DyFeO_3$ nanoparticles. The analysis shows that the components detected in measurements closely resemble the stoichiometric ratio of the theoretical formula $DyFeO_3$. The Dy/Fe atomic ratio at five different measured sites ranged from 0.95 to 0.98, verifying compositional homogeneity.

Fig3 shows the optical absorbance spectrum of the $DyFeO_3$ sample obtained from UV–Vis spectroscopy. The absorption is dominated by O 2p → Fe 3d charge-transfer (p–d) transition from the valence band of oxygen to the conduction band of iron[15]. The direct band gap was estimated from the absorption data using Tauc's method. For $DyFeO_3$, the direct band gap was found to be ca. 2.01 eV. The photocatalytic performance of $DyFeO_3$ particles was tested by tracking the degradation of five organic dyes, methyl orange (MO), rhodamine B (RhB), methylene blue (MB), and acid fuchsine (AF), with visible light irradiation. The photocatalytic process of the prepared $DyFeO_3$ nanostructures is depicted in Fig4a. While these colored dyes contain absorption bands in the visible spectrum, which can affect

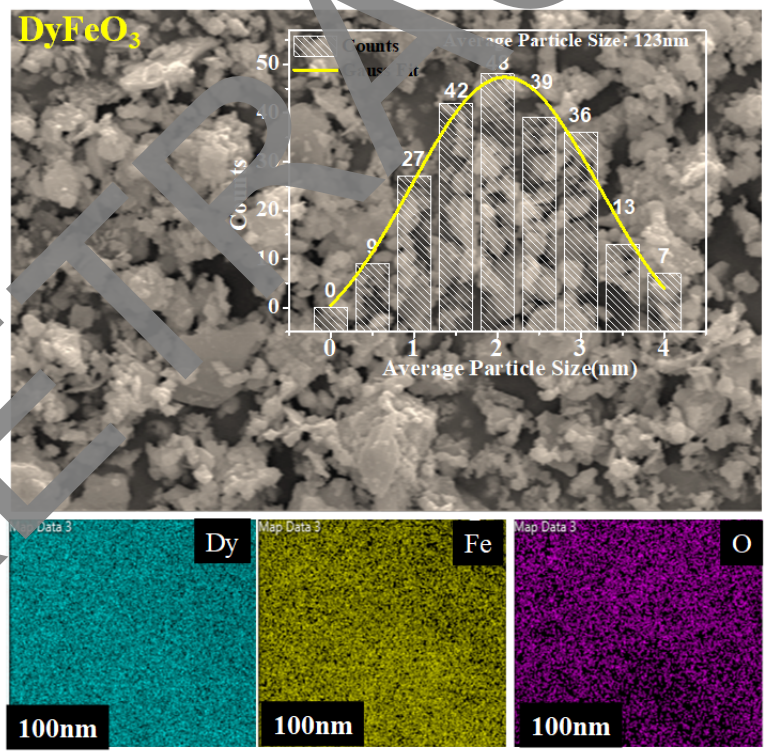

Figure 2. Surface morphology of $DyFeO_3$ nano particle, Average particle sizes and elemental distribution shown

Table 1. Structural refinement parameters of $DyFeO_3$ nano particle synthesized by sol-gel process

Compound: $DyFeO_3$	Crystal System: Orthorhombic		
	Space group: Pbnm		
	x	y	z
Dy	0.0677	0.25	0.484
Fe	0	0	0
O1	0.4573	0.25	0.5913
O2	0.3071	0.0584	0.109
Lattice Parameters	a(Å)	b(Å)	c(Å)
	5.5631	7.8516	5.553
$\alpha=\beta=\gamma=90^o$			
Unit Cell Volume(V) = 226.7695(Å)3			
Fitting Parameters	RWP(%)=6.31,RP(%)=5.21		

photocatalytic activity in that they (1) photosensitize the dyes and (2) screen some light from the catalyst, degradation of dyes by $DyFeO_3$ is a direct indicator of photocatalytic efficiency. The percentage degradation of the dyes after 6 hours of irradiation is presented in Fig4a, and also the result of the blank experiment. The percentage degradation is calculated as[16]:

$$D_e = \frac{C_0 - C_t}{C_0} * 100 \quad (1)$$

where (C_0) and (C_t) are the initial concentration of dye before and after irradiation, respectively. For the absence of $DyFeO_3$ particles, the dyes had negligible degradation, with MB

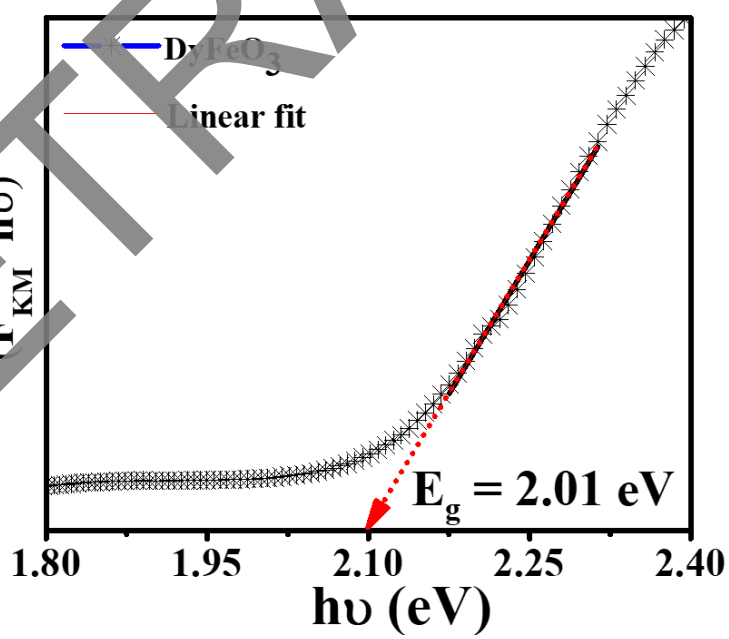

Figure 3. The optical band gap estimated with the help of Tauc's plot of $DyFeO_3$ nano particle synthesized by sol-gel process

having only 5% degradation in 6 hours, affirming their stability under visible light. With the addition of $DyFeO_3$ nanoparticles, comprehensive photocatalytic degradation of all the dyes was achieved. Under the current testing conditions (concentration of dye: 10 mg/L; dosage of catalyst: 1 g/L; natural pH), the decoloration efficiency was in the following order: AF > MB > RhB > MO. This difference is due to a number of reasons, among them the molecular structure of the dye and the adsorption affinity of the catalyst towards the molecules of the dye. Fig4b presents $\ln(C/C_o)$ versus irradiation time (t) plots for the four dyes. The kinetics of photodegradation can be well modeled by the first-order rate equation[17]:

$$ln\frac{C_t}{C_o}100\% = -KT \tag{2}$$

Where (kapp) is the apparent rate constant [31]. In each of these, the correlation coefficient (R2) was greater than 0.9, reflecting good agreement with first-order kinetics. The rate constants were in the same order as the efficiencies of degradation: AF > MB > RhB > MO.

4 Conclusions

In summary, $DyFeO_3$ perovskite nanoparticles with an orthorhombic structure (space group Pbnm) were successfully synthesized and systematically characterized. XRD analysis combined with Rietveld refinement confirmed the formation of a single-phase material with lattice parameters of a = 5.5631 Å, b = 7.8516 Å, and c = 5.5530 Å, and an average

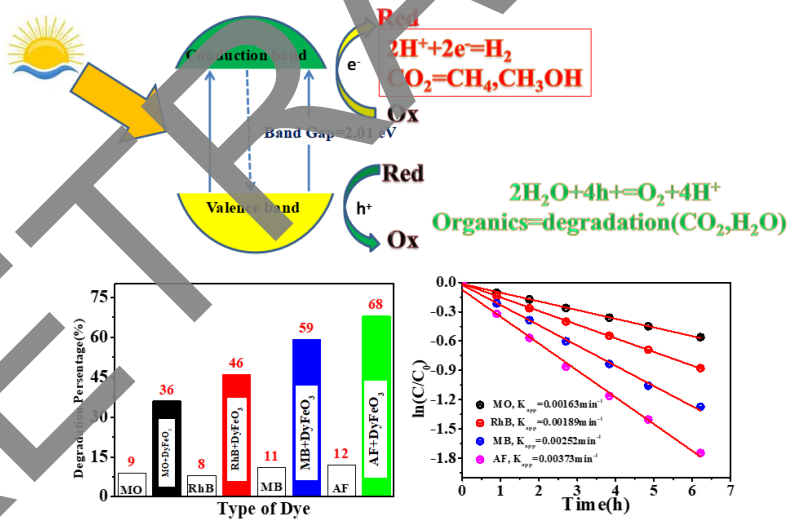

Figure 4. (a) Schematic representation of the visible-light-driven photocatalytic mechanism of $DyFeO_3$ nanoparticles, showing the generation of electron–hole pairs, formation of reactive oxygen species (•OH, O_2^-), and subsequent degradation of organic dyes. (b) Photocatalytic degradation of methyl orange (MO), rhodamine B (RhB), methylene blue (MB), and acid fuchsine (AF) over $DyFeO_3$ nanoparticles under visible-light irradiation, indicating percentage degradation after 6 h. The blank experiment confirms negligible degradation in the absence of the catalyst. (c) First-order kinetic plots of $\ln(C/C_o)$ versus irradiation time (t) for the four dyes, illustrating the photocatalytic rate constants and confirming first-order degradation kinetics

crystallite size of approximately 136 nm. SEM observations revealed non-isometric particles with an average particle size of about 123 nm, exhibiting a tendency toward agglomeration, while EDX analysis verified the stoichiometric elemental composition and good chemical homogeneity. Optical studies indicated a direct band gap of 2.01 eV, attributed to O 2p → Fe 3d charge-transfer transitions. The DyFeO3 nanoparticles demonstrated excellent visible-light-driven photocatalytic performance, effectively degrading various organic dyes (AF, MB, RhB, and MO) following pseudo-first-order kinetics, with degradation efficiency influenced by dye molecular structure and adsorption affinity. Overall, these results establish $DyFeO_3$ nanoparticles as optically active, structurally stable, and efficient visible-light photocatalysts, highlighting their potential for environmental remediation and other advanced functional applications.

ACKNOWLEDGMENTS

The authors, V.S. Noorjahan Begum and Dr. DZarena, extend their sincere gratitude to Dr. Prabhakar for his invaluable assistance with the structural refinement.

Data Availability Statements

The authors declare that all the data generated or analyzed during this study are included in this manuscript.

Author Contributions

V.S. Noorjahan Begum: Investigation, methodology, Data curation,writing draft and data validation.Dr. D. Zarena: Conceptualization, supervision, and review and writing the manuscript.

Conflict of Interest

The authors declare that they have no known competingfinancial i nterests o r personal relationships that could have appeared to influence the work reported in this paper.

References

[1] Parida, Bichitra Nanda et al., Effect of rare-earth elements on perovskite composite materials. Perovskite Metal Oxides 253–272 (2023).

[2] Ahmad, Naseem et al., A comprehensive study of structural, electrical and ferroelectric properties of NdFeO3-SnO2 nanocomposite. Physica Scripta **97**, 115819 (2022).

[3] Zhao, ZY et al., Ground state and magnetic phase transitions of orthoferrite DyFeO 3. Physical Review B **89**, 224405 (2014).

[4] Khan, Huma et al., Emerging rare earth perovskite nanostructures for efficient electrochemical energy conversion and storage. International Journal of Hydrogen Energy **58**, 954–963 (2024).

[5] Tarek, Mohasin et al., Nanostructured DyFeO 3 photocatalyst: an authentic and effective approach for remediation of industrial and pharmaceutical wastewater. Journal of Materials Chemistry A **12**, 25475–25490 (2024).

[6] Wu, Jhen-Yang et al., Tunable photocatalytic properties of Au-decorated BiFeO3 nanostructures for dye photodegradation. ACS Applied Nano Materials **7**, 9777–9788 (2024).

[7] Danks, Ashleigh E et al., The evolution of 'sol–gel'chemistry as a technique for materials synthesis. Materials Horizons **3**, 91–112 (2016).

[8] Bokov, Dmitry et al., Nanomaterial by sol-gel method: synthesis and application. Advances in materials science and engineering **2021**, 5102014 (2021).

[9] Florea, Ana-Maria et al., Solid-State Materials for Opto-Spintronics: Focus on Ferromagnets and 2D Materials. Solids **6**, 25 (2025).

[10] Mishra, Rahul et al., Emerging spintronics phenomena and applications. IEEE Transactions on Magnetics **57**, 1–34 (2020).

[11] Ismael, Mohammed et al., Solid state route for synthesis of YFeO3/g-C3N4 composites and its visible light activity for degradation of organic pollutants. Catalysis Today **313**, 47–54 (2018).

[12] Jabbarzare, Saeid et al., Mechanochemically assisted synthesis of yttrium ferrite ceramic and its visible light photocatalytic and magnetic properties. Journal of Alloys and Compounds **688**, 1125–1130 (2016).

[13] Lone, Irfan H et al., Multiferroic and photocatalytic properties of DyFeO3 nanoparticles stabilized by citrate precursor route. Bulletin of Materials Science **47**, 48 (2024).

[14] Brahlek, M et al., Structural refinement of Pbnm-type perovskite films from analysis of half-order diffraction peaks. Journal of Applied Physics **121**, (2017).

[15] Lad, Robert J et al., Photoemission study of the valence-band electronic structure in Fe x O, Fe 3 O 4, and $$-Fe 2 O 3 single crystals. Physical Review B **39**, 13478 (1989).

[16] Phinikarides, Alexander et al., Review of photovoltaic degradation rate methodologies. Renewable and Sustainable Energy Reviews **40**, 143–152 (2014).

[17] Valente, José, Studies on the adsorption and kinetics of photodegradation of a model compound for heterogeneous photocatalysis onto TiO2. Chemosphere **64**, 1128–1133 (2006).